

Cuffless blood pressure estimation based on composite neural network and graphics information

Ye Qiu^a, Dongdong Liu^a, Guoyu Yang^a, Dezhen Qi^a, Yuer Lu^a, Qingzu He^a, Xiangyu Qian^a, Xiang Li^a, Yuping Cao^{b,*}, Jianwei Shuai^{a,c,*}

^a Department of Physics, and Fujian Provincial Key Laboratory for Soft Functional Materials Research, Xiamen University, Xiamen 361005, China

^b Department of Psychiatry of Second Xiangya Hospital, Central South University, The China National Clinical Research Center for Mental Health Disorders, Changsha 410011, China

^c National Institute for Data Science in Health and Medicine, and State Key Laboratory of Cellular Stress Biology, Innovation Center for Cell Signaling Network, Xiamen University, Xiamen 361102, China



ARTICLE INFO

Keywords:

Blood pressure (BP)
Electrocardiography (ECG)
photoplethysmography (PPG)
Cuffless BP prediction
Compound neural network
Deep learning

ABSTRACT

Blood pressure (BP) assessment and dynamic detection are of great significance for timely detection of the morbidity of hypertension, which is a major risk factor for most cardiovascular diseases (CVDs). It has been proved that the dynamic BP can be effectively predicted by using the combined input of photoplethysmogram (PPG) and electrocardiographic (ECG) signals. In this paper, we proposed a hybrid neural network architecture, which contains CNN-Sequential-Adapt layer, ResNet25_BP layer with squeeze and excitation (SE) block and fully connected layers, for BP estimation. The structure based on the convolutional network aims at the current inputs, which can effectively absorb the graph information of the inputted biological signals and make the model more stable and reliable. We evaluated the performance of two datasets including 1216 and 40 subjects, based on the criterions of British Hypertension Society (BHS) and the Association for the Advancement of Medical Instrumentation (AAMI). According to the BHS and AAMI standards, the outputs of the model achieved grade A on BHS and met the AAMI criteria. The mean absolute errors (MAE) of systolic BP and diastolic BP are 3.70 and 2.81 mmHg in the large dataset, and 1.37 and 0.93 mmHg in the small dataset, respectively.

1. Introduction

Cardiovascular diseases (CVDs) including hypertension and arrhythmia are the main causes of death worldwide, especially for the elderly living in countries that do not have adequate medical treatments [1]. The risk of CVDs has shifted to the young people who have been sub-healthy and inactive in the past few years. The occurrence of CVDs is usually sudden and fatal. Monitoring of blood pressure (BP) is considered as one of the necessary methods to avoid CVDs caused by the variation of BP [2].

The clinical noninvasive methods of BP measurement are mainly used by the blood cuff, including auscultation, oscillometry and volume clamping [3]. These BP measurement methods have been lasted for a long time and have some limitations, such as discontinuity and inconvenience. Obviously, these methods cannot be used to monitor the continuous BP of patients. Meanwhile, the invasive methods that can measure BP continuously were only used in patients who have serious

disorder and medical observation in intensive care unit. The invasive methods are the gold standard, but cannot be the mainstream method because its cost is unacceptable for people without serious illness. Due to medical needs, simple continuous BP monitoring methods are urgently needed to be applied in clinical diagnosis.

The cost of continuous BP detection will be greatly reduced if BP can be obtained by correlating it with some biological signals which are easily detectable, such as photoplethysmography (PPG) and electrocardiograph (ECG). Previous works have proved that BP can be effectively predicted by using the combined PPG and ECG. The ECG and PPG which are easy to obtain from the wearable device or instrument have become the signals to estimate BP in recent decades [4,5].

In the early applications of these signals, the pulse wave velocity (PWV) and the pulse transit time (PTT) were used to build a complex linear or nonlinear relationship with BP [6,7]. The relationship between BP and pulse wave has been studied for a long time. Mukkamala et al. used a model for the relationship between PTT, age, and sex and BP to

* Corresponding authors at: Department of Physics, Xiamen University, Xiamen 361005, China.

E-mail addresses: caoy001@csu.edu.cn (Y. Cao), jianweishuai@xmu.edu.cn (J. Shuai).

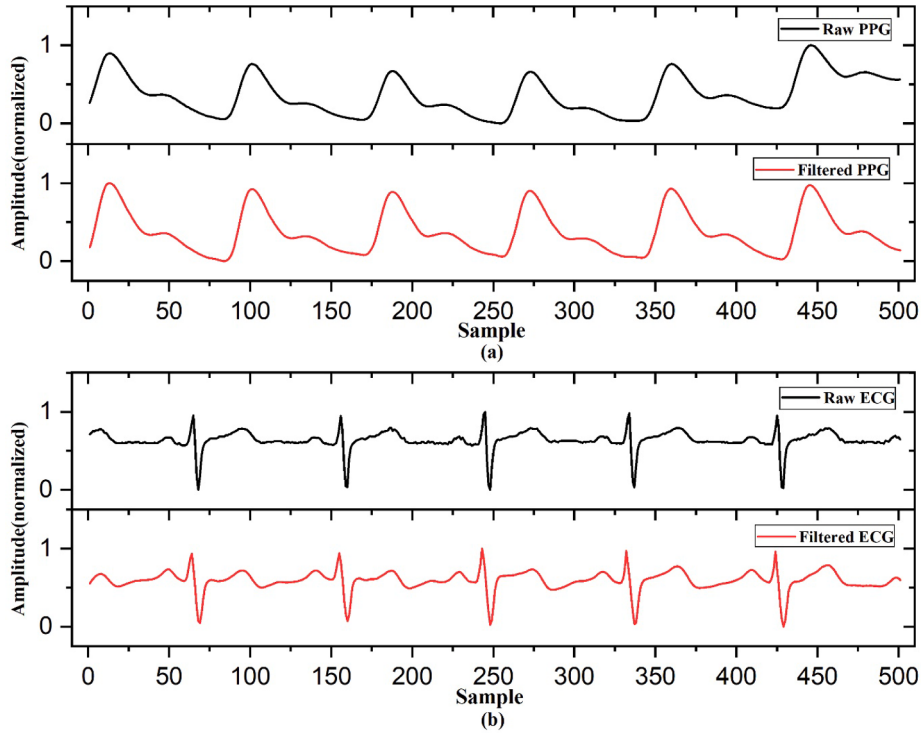


Fig. 1. Comparison of PPG (a) and ECG (b) signals before and after filtering. The baseline drift and the high frequency noise in the signals are removed effectively.

determine the PTT-BP calibration curves for each age and sex [8]. Singla et al. adopted wavelet transform on ECG and PPG signals, and estimated BP value through the joint detection of these signals [9]. Pulse arrival time (PAT) that is defined as the time delay from the R-peak of ECG to the next trough of PPG during a specific period was also considered as a parameter to estimate BP [10]. Liu et al. studied the information based on the waveform of PPG and estimated BP with multiple regression model [11]. A method based on the combination of PPG signals morphology and ECG was proposed by Li et al. [12]. Shin et al. simplified the PPG waveform by using an approximate model and then analyzed it as blood flow velocity and acceleration using the derivative of PPG with the pressure index (PI) introduced as a new factor [13].

Recently, the machine learning (ML) methods were also applied in the field of cuffless BP estimation based on the clinical data or the relevant physiological signals [14]. Early ML methods typically used logistic regression analysis, support vector machine (SVM) and other methods based on the manually selected feature extraction. Features selected from PPG signals include the width of the 1/2 and 2/3 amplitudes, the foot extracted PAT, the midpoint and peak value, the systolic upstroke time, and the diastolic time [15]. The eigenvalues, such as the Womersley number, were also suggested as feature inputs which contained information of waveform for BP estimation [16]. Kachuee et al. discussed a ML method to extract feature values from PPG and then predict BP with SVM [17]. Kachuee et al. also proposed a framework of AdaBoost which consists of 1000 decision trees for BP estimation with the extraction of two types of features [18]. Ding et al. improved the accuracy of long-term BP monitoring by introducing new indicators, photoplethysmogram intensity ratio (PIR), into the regression model [19]. Lin et al. extracted nineteen eigenvalues based on PPG and PTT on a small sample and estimated BP using the linear regression [20]. Feng et al. proposed a ML strategy based on the regularized linear regression (RLR) to construct BP models with different covariates for the corresponding groups on 28 subjects. The RLR of the individual was used as the initial calibration, and the recursive least squares method was used for re-calibration [21]. Hassani et al. applied a nonlinear mapping to reduce the size of the feature vector by mapping the input parameters to

a potential space, used a multi-stage noise reduction technique to effectively smooth the input signals, and then considered SVM to estimate BP values [22]. By evaluating the correlation between various characteristic points and BP, it was found that the diastolic time (DT) which can be computed by the distance from the peak to foot of PPG has a high relevance with BP [23]. Hu et al. used a single-channel PPG signals to estimate systolic BP (SBP) and diastolic BP (DBP) by an integrated ML algorithm of XGBoost [24].

Due to the specificity of the biological signals from the individual bodies, the features extracted from morphology are usually error prone. Furthermore, the morphological features with manual selection may have a good performance, but the ML-based methods need the professional medical knowledge to set up the rule-making formula [25]. Thus, different from the above statistical rule-making ML methods, the deep learning (DL) technology was applied to BP estimation, which abandons the statistical rule-making processes. A hybrid neural network model based on the mean impact value and genetic algorithm was discussed for BP prediction from PPG signal [26]. Tanveer and Hasan used the fully connected layer and LSTM layer neural network to predict BP on a small sample [27]. Slapničar et al. took the PPG and its first and second derivatives as inputs into a spectral-temporal deep neural network with residual connections to mimic the dependence between PPG and BP [28]. A composite network structure using convolutional neural network (CNN) and LSTM was proposed by JEsmalpoor et al. in which the CNN layer was used to extract eigenvalues, and then sent to LSTM for BP estimation based on temporal variation [29]. Eom et al. proposed a model consisted of CNN, a bidirectional gated recurrent unit, and an attention mechanism [30]. Through the experimental comparison, it was found that the model with attention mechanism shows better performance for BP prediction. Aguirre et al. discussed a cuffless method to estimate the morphology of the arterial BP through a deep learning model based on a seq2seq architecture with attention mechanism [31]. Beyond the BP prediction, the deep neural network is also able to diagnose various diseases, such as diabetes and congestive heart failure, by inputting various biological signals, such as blood glucose concentration, diastolic BP, body mass index, heart rate variability [32,33].

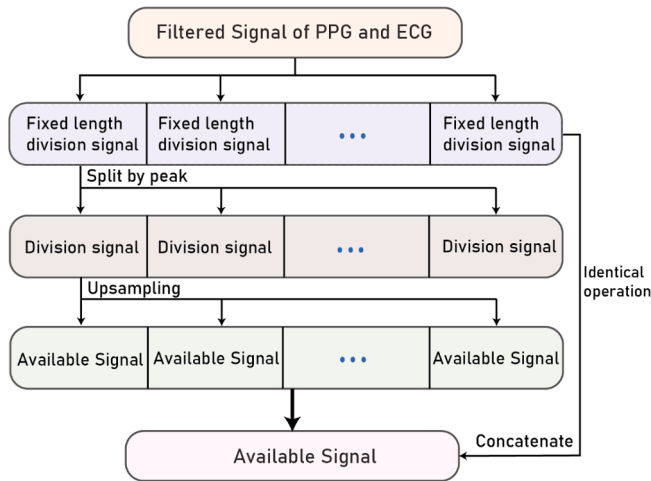


Fig. 2. Pre-processing flow chart of signals from the original filtered signal of PPG and ECG to the available signals, each filtered signals are processed with the same operation.

In this work, we focus on the feature value extraction based on graphics information of PPG and ECG, and adopt a carefully designed feature extraction structure, which is more suitable for a better BP prediction with large subject databases. In our model, the input signals are treated as an overall picture, in which the length is the size of the signal segment, and the width is the number of signal types. We consider PPG and ECG as two-dimensional data from the same channel. The CNN is used to compute the hidden features of PPG and ECG, which can replace the artificial feature extraction. In the [Section 1](#), we mainly review the various methods in the field of cuffless BP estimation, including linear correlation, ML and DL models, and propose a new perspective to deal with PPG and EEG. The main content of the [Section 2](#) is the signals preprocessing, the structure of proposed model and the specific experimental details. The comparison of statistical results of the models is described in the [Section 3](#). Discussions and conclusions about the results and the performance of the model are put forward in the [Section 4](#) and [5](#) respectively.

2. Materials and method

In this section, we describe the preprocessing phase including data slicing and resampling and introduce a more robust model structure to extract features effectively. The data extracted from the Multiparameter Intelligent Monitoring in Intensive Care (MIMIC-II) database [34] include PPG, ECG and ambulatory blood pressure (ABP).

2.1. Preprocessing

2.1.1. Noises filtering

The signals extracted from the database are not completely clean and require filtering process, including filtering the high-frequency noise and the low-frequency noise to get rid of the baseline drift. The original and filtered signals are shown in Fig. 1. Some noises that may affect model learning are filtered out.

2.1.2. Cutting signals through sliding window

The filtered signals are cut into a set of unified segments by a non-overlapping sliding window. The reason to use the size-fixed window for data process is that this method can avoid the cutting error of the whole waveform caused by unique points and make more effective use of filtered data to generate usable datasets. The signal resulting from the window is further processed using cutting by peak and resampling. Since the input of two signals is regarded as two-dimensional data on the same channel, adopting the same data cutting mode will make them more

unified. Meanwhile, the fixed number of peaks will ensure that the convolution layer extracts the same morphological features from the input signals. For patients, if a window of fixed length is used to cut the signals, the number of periodic cycles contained in individual length-fixed window is uncertain due to the different heart rates [27]. As a result, each input signal has approximately the similar waveform information and does not have different input periods depending on the patients' heart rate. It is easier for the model to learn the different characteristics of each input signal for estimation.

2.1.3. *Signal shuffle*

All the size-fixed signals for all the subjects are randomly stored in the database, without the object information and the time series information in the original PPG and ECG signals. The training and testing datasets consist of the segments from all the objects, respectively. As a result, the model can learn the features for all the objects with the training dataset. Since our model does not contain the recurrent neural network module which has the memory unit, all the size-fixed signals in the training dataset can be randomly put into the model for training. This procedure of time-independent makes the model to focus on the extraction of the graphic information of input signals in real time. This preprocessing method provides more possibilities for the dataset to combine the input signals.

2.2. Pretreatment experiment process

First, we extract N subjects that contain enough length. The length of each sample satisfies the requirement of train and test. The datasets of each subject are divided into 70% and 30% fragments for train and test, respectively.

Second, the data from the different subjects are cut into fragments with $everyH = 1000$ points. Formally, the data for each subject will be separated to K segments. As a fact, if the peaks have a mistake of recognition which may be produced by the intensive interference from acquisition equipment, the whole anchor point will not be changed significantly. The original sampling rate was 125 Hz and so $everyH = 1000$ points represent 8-second length of fragment for PPG and ECG signals.

Third, within the H points, there are U consecutive peaks corresponding the R-peak of ECG and the systolic peak of PPG. Every three peaks are extracted for the next preprocessing stage.

Fourth, the extracted signals are resampled by the fixed P points for model and processed by min–max normalization.

The bound of ABP is extracted by the widest range of PPG and ECG in one period. Formally, if the bound of PPG and ECG is $[x_1, x_n]$ and $[y_1, y_n]$, respectively, the bound of label is considered as

$$Ra = [min(x_1, y_1), max(x_n, y_n)] \quad (1)$$

This extracting method can ensure the correspondence of each input and output. For pursuing the consistency of each input model, each periodic input will be resampled to a certain value P . In this work, P was set to 513, which can make convolution kernel more efficient. Then, the input format of X_i is defined as

$$X_i = 513*2 \quad (2)$$

The input X_i are defined as sequence which has two dimensions of information. We adopted the ideas in the field of image processing and regarded two signals of PPG and ECG as one picture for processing. The signals flow chart of pretreatment is shown in Fig. 2.

Both PPG and ECG signals go through the above processing steps. It is noteworthy that these steps can improve the ability of model to extract features. Finally, the number of available fragment signals after above procedure is given by

$$A_{signals} = N^* \left(K^* \frac{U}{3} \right)^* 2 \quad (3)$$

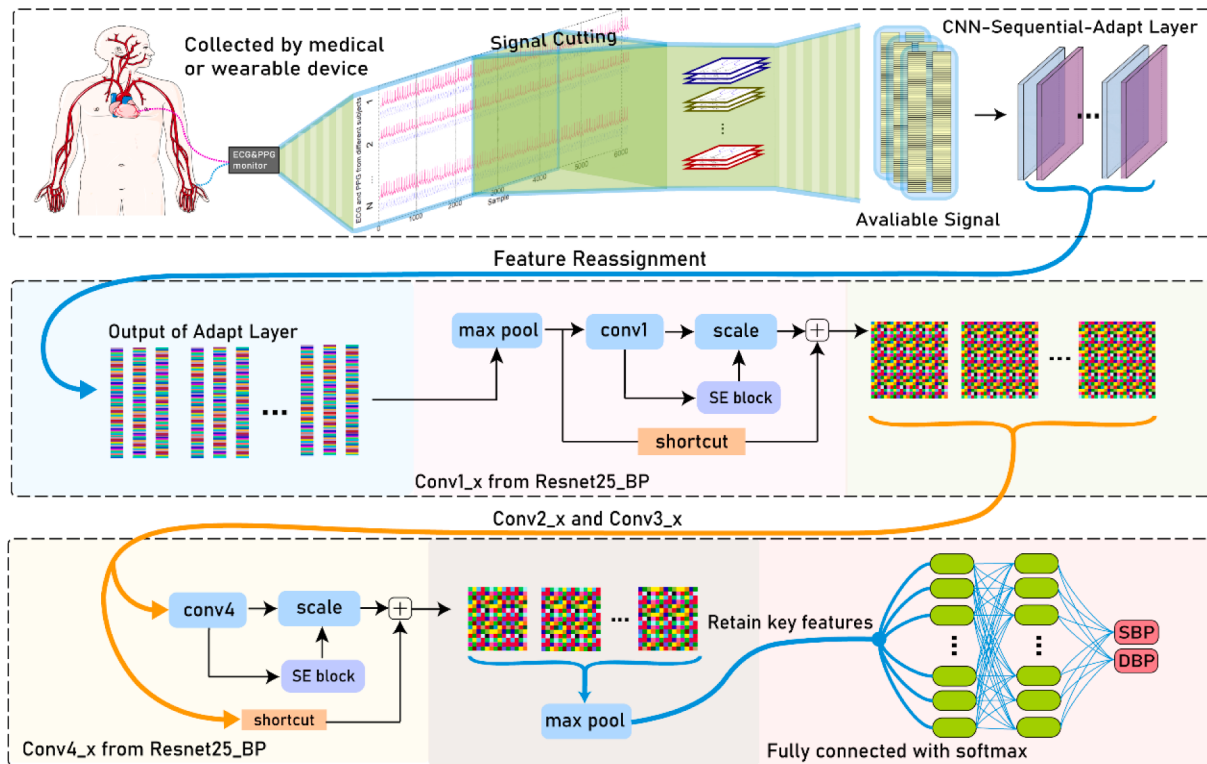


Fig. 3. Holistic feature information flow and an overview of the proposed model framework, including the CNN-Sequential-Adapt layer, ResNet25_BP, the added SE-block structure, and finally the fully connected layer. Specific model structure parameters are given in Table 1.

Table 1
Parameters of ResNet25_BP.

layer name	output size	ResNet25_BP
conv1_x	114 × 114	3 × 3 max pool, stride 2 1 × 1, 4 3 × 3, 4 × 2 1 × 1, 16
conv2_x	57 × 57	1 × 1, 8 3 × 3, 8 × 2 1 × 1, 32
conv3_x	29 × 29	1 × 1, 16 3 × 3, 16 × 2 1 × 1, 64
conv4_x	15 × 15	1 × 1, 32 3 × 3, 32 × 2 1 × 1, 128 1 × 1 average pool, 2-d fc, soft max

Every single array of input corresponds to the ground truth, which are extracted by the range of R_a in ABP.

2.3. Proposed model

In this paper, the model structure with CNN modules can effectively enhance the ability of describing features when the subjects have various forms. Squeeze and excitation (SE) block is also considered as a tool of enhancement for BP predication.

Because ECG and PPG are considered as the same channel on the convolution layers, the model can simultaneously extract the eigenvalues of the two sequences and integrate the features into the next convolution. Thus, the extracted morphological information of the channels contains two dimensional sequences effectively. The proposed model is composed of CNN-Sequential-Adapt layer, residual network 25-layer for BP (ResNet25_BP), SE block and fully connected layer. The SE block can reinforce the features extracted from the ResNet25_BP through

the channel attention mechanism, and then the fully connected layers with SoftMax are used to integrate the information extracted from the previous module.

2.3.1. CNN-sequential-adapt layer

Due to the ResNet structure was originally designed for the classification of images with uniform length and width, the input needs to adapt to a fixed format. The CNN-Sequential-Adapt layers which contains the convolution layer, batch-normalization (BN) layer, and Max pooling layer are designed to generate the appropriate output for ResNet25_BP. The convolution kernel size of the adaptive layer needs to accommodate the above feature points of PPG and ECG. Based on the resampling size of 513 and the receptive field, the kernel size of adaptive layer is set to 64. The existence of square convolution kernel requires the length of sequence to meet the uniform length and width. Through the elaborate parameters of the adaptive layers, the ResNet25_BP can extract features effectively from waveforms of PPG and ECG.

2.3.2. ResNet25_BP

The residual neural networks are widely used in target classification and other fields, as well as a part of classical neural networks, being the backbone of computer vision tasks [35,36]. The main proposed networks are ResNet50, 101, and 152 [37]. The advantage of this structure is that it is easy to optimize and the accuracy can be improved by increasing the depth of model. Its network structure also shows good stability and accuracy in one-dimensional signals processing [36]. The key conception of ResNet is the shortcut which can solve problem of gradient vanishing caused by increasing depth in deep neural network.

The residual network is composed of a series of residual blocks which are shown in Fig. 3. Formally, the output without the residual is denoted as $H(x)$, and the input that corresponding to residual is X_i . Then, the final output is defined as

$$X_i + 1 = \text{relu}(H(X_i) + \text{identity}(X_i)) \quad (4)$$

Table 2

Comparative statistical analysis on the different number of input signals and the selection of SE block.

Model	Number of input signal J = 8				Number of input signal J = 16				Number of input signal J = 32			
	SBP		DBP		SBP		DBP		SBP		DBP	
	MAE	RMSE	MAE	RMSE	MAE	RMSE	MAE	RMSE	MAE	RMSE	MAE	RMSE
Without SE block	5.68	7.83	4.11	5.76	5.15	7.11	3.85	5.34	4.69	6.36	3.53	4.81
With SE block	4.75	6.65	3.44	4.99	4.20	5.87	3.13	4.53	3.70	5.11	2.81	3.95

Table 3

The performance of the proposed model on AAMI.

	ME	STD	Subjects
Required Deviation	<5 mmHg	<8 mmHg	>85
Systolic Blood Pressure	0.18	5.11	1216
Diastolic Blood Pressure	0.01	3.95	1216

Table 4

The performance of the proposed model on BHS.

Cumulative Frequency of Error	<5 mmHg	<10 mmHg	<15 mmHg
Grade A	60%	85%	95%
Grade B	50%	75%	90%
Grade C	40%	65%	85%
SBP prediction(J = 16) without SE-block	61.07%	86.72%	95.48%
DBP prediction(J = 16) without SE-block	73.65%	94.28%	98.20%
SBP prediction(J = 16) with SE-block	70.61%	91.85%	97.78%
DBP prediction(J = 16) with SE-block	82.17%	96.22%	98.80%
SBP prediction(J = 32) without SE-block	63.93%	89.81%	97.59%
DBP prediction(J = 32) without SE-block	76.37%	95.48%	99.15%
SBP prediction(J = 32) with SE-block	76.01%	94.33%	98.70%
DBP prediction(J = 32) with SE-block	85.41%	97.15%	99.52%

The original mapping is recast into $H(X_i) + X_i$. The structure of shortcut which takes the original input to output directly without convolution calculation makes the model easier to optimize the residual mapping than the unreference mapping. Because the original intention of ResNet was to solve the issue of image classification which has plentiful information than two dimensional biological signals, the specific parameters are adjusted to adapt the biological information from the adaptive layer. The variation of channel is designed from 1 to 128, which is used to prevent the overfitting caused by the complicated model. The calculation of $H(X_i)$ is composed by three weight layers that contain BN layers and convolution layers.

The detailed parametric setting and network structure of ResNet25_BP are shown in Table 1 and Fig. 3, respectively. Finally, the fully connected layer with the activation function and the average pool is used to integrate the output from the ResNet25_BP.

2.3.3. SE block

The SE block is not a complete network structure, it can be understood as an attention mechanism which can improve the interdependency between channels. It was considered as an effective way to promote the ability of CNN modules. In our model, we replaced the original residual blocks by the blocks with SE structure, as shown in Fig. 3. With SE block, the weight of channel from the ResNet25_BP layer is redistributed based on the global information. As the channel characteristics are recalibrated, it selectively enhances the useful information and suppresses the useless information [38].

The whole operation steps are given as follows. First, the global average pooling is used to compress the spatial dimension features, and the same number of channels as the input is considered for the output.

After squeeze, each independent feature channel typically contains the global information. Secondly, the excitation step generates the weight parameters for each feature channel to explicitly set up the correlation between feature channels. The third step is to reweight the model parameters. The weight parameters of the output reflect the importance of each feature channel. The scale layer operation is to weight the previous channel-by-channel feature to complete the recalibration of the original feature on the channel dimension. Through these processes, the attention mechanism on the channel can effectively extract the useful features and perform BP calculations. For reducing the number of parameters, the ratio r is set to 16.

2.4. Statistical methods

According to the requirement of the Association for the Advancement of the Medical Instrumentation (AAMI) and British Hypertension Society (BHS), the mean error (ME), the mean absolute error (MAE) and the root mean square error (RMSE) are used to evaluate the performance of the proposed model. The definition of ME, MAE and RMSE are given as follows

$$ME = \frac{1}{N} \sum_{i=1}^N (P_i - Y_i) \quad (5)$$

$$MAE = \frac{1}{N} \sum_{i=1}^N |P_i - Y_i| \quad (6)$$

$$RMSE = \sqrt{\frac{1}{N} \sum_{i=1}^N |P_i - Y_i|^2} \quad (7)$$

in which P_i and Y_i represent the prediction from the model and the ground truth from the golden standard. ME is the general estimation ability of a model, which is determined by the average value of each error. The use of RMSE helps to provide a complete image of the error distribution. MAE can avoid the situation that the errors cancel each other, so it can accurately reflect the actual prediction error. Additionally, the statistical parameter of Pearson's correlation coefficient (R) is also used to evaluate the correlation between the prediction and ground truth, which is given by

$$R = \frac{\text{corr}(X, Y)}{\sigma_x \cdot \sigma_y} \quad (8)$$

3. Result

Since the gold standard of BP value is determined by the invasive method, the evaluation standard of BP calculated by PPG and ECG is to minimize the error between the estimation performance and the invasive BP. For evaluating the reliability of the proposed model, we extract 1216 and 40 records containing many of waveform information from the database, respectively. The advantage of the model proposed in this paper is that it can extract macro features. Thus, the analysis of the statistical results will focus on the dataset with more samples. Since the hemodynamic information of each sample is unique, analyzing the cycle morphology also confirms that the same waveform may correspond to the different BP values. As a result, each subject will provide part of the

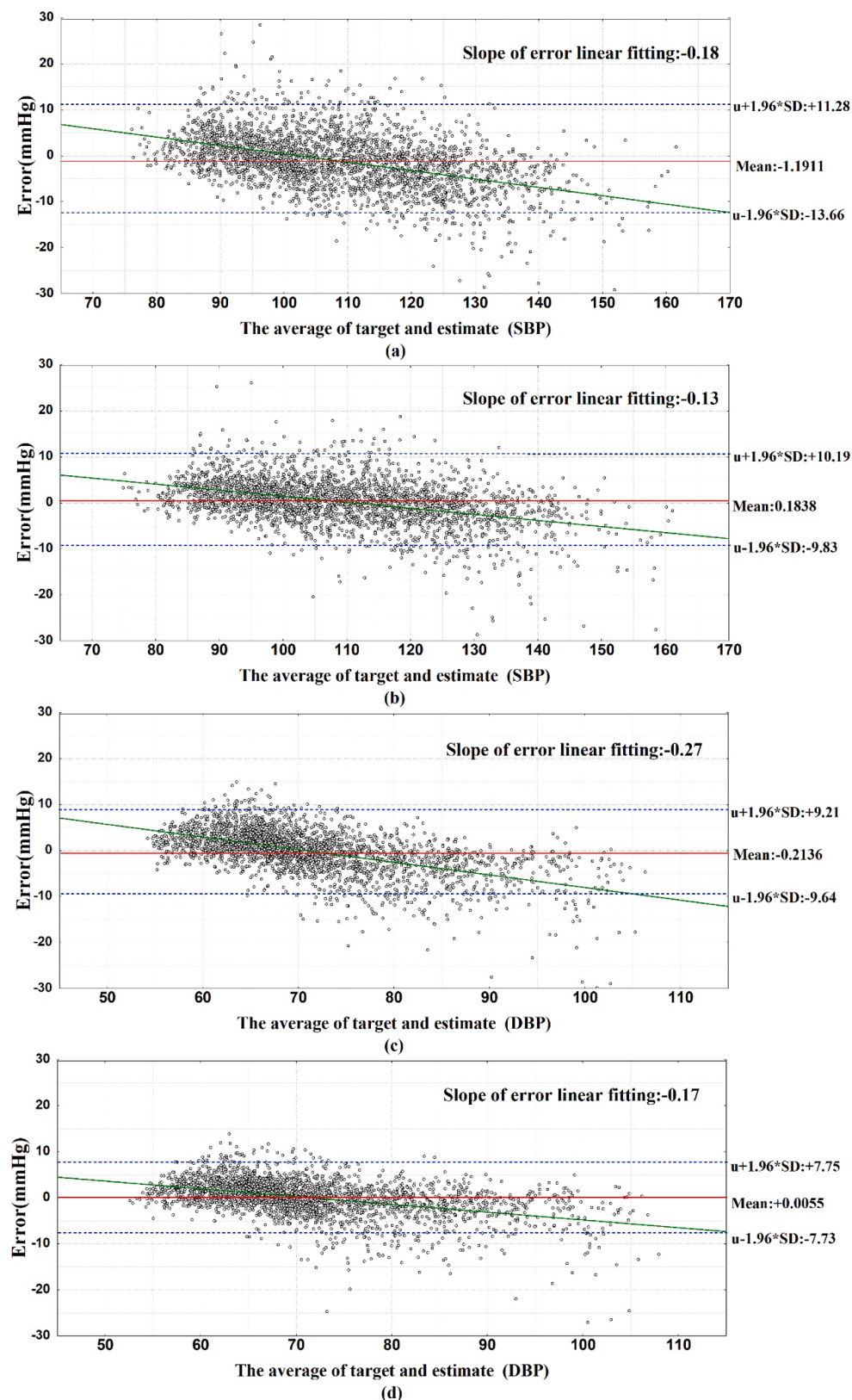


Fig. 4. Bland-Altman plots of SBP (a) and DBP (b) without SE blocks and SBP (c) and DBP (d) models with SE blocks. The green line is a linear regression analysis of errors.

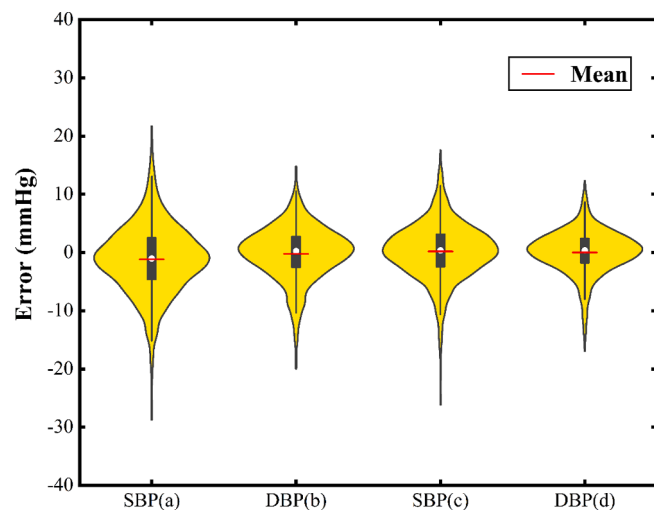


Fig. 5. Violin plots of SBP (a) and DBP (b) errors for models without SE block and SBP (c) and DBP (d) with SE block, where the red line is the mean value of the error.

data for training [20,27,29,39]. This classification method ensures that the model can extract enough feature information for each subject, because the model needs to extract the intrinsic features for each subject which has the unique hemodynamic information.

As described in Section 2.1.3, the signals which have the information of different graphics are imported to the model at the same time. The signals imported into the model can even come from the different subjects. The ability to rely entirely on the current graphics input can be used for patients who have the unstable PPG or ECG. In order to evaluate the performance of the model with different number J of input signals, we tested the performance of model when different amounts of input are fed, including $J = 8, 16, 32$.

To test the effect of the SE block on the model, we counted the model output with and without the block. Specific indicators are shown in Table 2. The MAE for SBP and DBP are 3.70 mmHg and 2.81 mmHg. As can be seen from Table 2, when $J = 32$, after adding the SE block module to the residual block, the MAE value of SBP is reduced from 4.69 mmHg to 3.70 mmHg, and the MAE value of DBP is reduced from 3.53 mmHg to 2.81 mmHg.

In order to further evaluate the performance of the model, the value of ME and standard deviation are given in Table 3 with the mean and standard deviation of estimation error for SBP and DBP 0.18 ± 5.11 mmHg and 0.01 ± 3.95 mmHg, respectively.

3.1. Performance evaluation on AAMI

The standard of AAMI requires ME and standard deviation values lower than 5 mmHg and 8 mmHg, respectively. The proposed model meets the AAMI criteria in all cases of the experiment. Table 3 presents the concrete performance of the best results of the proposed model, showing that the statistical parameters still meet the standard when the number of subjects is larger than the requirement.

3.2. Performance evaluation on BHS

The standard of BHS presents grades A, B and C based on the cumulative frequency percentage errors MAE less than three different thresholds, i.e., 5, 10, and 15 mmHg, respectively [40]. The evaluation criterion based on BHS standard is assessed on the number of input signals J and the selection of SE block. When the number of input signals $J = 16$ and 32, the result of the proposed model satisfies the requirement of grade A. The specific data are given in Table 4.

3.3. Statistical analysis

The Bland-Altman diagrams of performance from the model with and without SE are presented in Fig. 4. Its underlying idea is to calculate the consistency limit of two sets of measurement results, and intuitively reflect this consistency limit with images. If the scatter points are uniformly distributed in the standard deviation line and the mean value is close to zero, the measurement result is better. Our results indicate that, with the linear regression analysis of Bland-Altman plot, the slope of linear fitting increases to a certain extent and the errors keep decreasing after adding SE block to the model. The slope of error linear fitting is shown in the upper right corner of each subfigure in Fig. 4, showing the effectiveness of adding modules for further calibration.

Violin Plot is used to show the distribution state and probability density of multiple groups of data. This chart combines the characteristics of a box chart and a density chart, which is mainly used to show the shape of errors distribution in this study. As shown in Fig. 5, by observing and comparing the violin plots of SBP and DBP errors, it can be found that the errors of the two plots are almost concentrated near zero, and the boundary is relatively smooth, indicating that the model performs better with SE block.

The regression plot is used to evaluate the linear relationship between the predicted value and the actual value. When the predicted result is better, the linear relationship between the two data is stronger. As shown in the contrast of Fig. 6, the Pearson's correlation coefficient R increases when the residual block adds the SE block, which can improve the convolution performance by redistributing the weight of channel from feature map. The box plot is mainly used to reflect the distribution characteristics of the original data, providing key information about the location and dispersion of the data. In this study, it mainly reflects the differences between the true values and predicted results in SBP and DBP.

The box plots of estimation error for the selection of SE block are shown in Fig. 7. The upper and lower horizontal lines correspond to the upper and lower edges of the box graph respectively, and the red cross marks indicate the abnormal values of the data. The horizontal line in the middle of the box represents the median point of the data. Fig. 7 shows that the model after excluding outliers performs better.

3.4. Comparison with previous work

In this study, the accuracy and statistical information of the model are evaluated on both large subjects (1216) and small subjects (40). Due to the influence of the main structure of the model, the performance on large samples is more noteworthy. In this paper, we used convolution module structure because of its theoretical support based on graphic information. Table 5 is a list of the results from the previous researches on cuffless BP estimation. Because the sample databases used in previous studies are not the same, even if the same database is used, the samples extracted may not be completely consistent. As a result, the results given in Table 5 only presents a statistical comparison.

4. Discussion

In this paper, we proposed a composite neural network consisting of CNN-Sequential-Adapt layer, Renet25_BP layer with SE block, and fully connected layers. Inspired by ML in the field of cuffless BP estimation, this paper innovatively proposed a completely graph-based neural network structure for BP prediction. The first layer of the compound neural network transforms the initial input graph information into the input shape that can be accepted by Renet25_BP layer. The accuracy improvement effect is explored when the network structure has SE block or not.

In interpretability, the CNN-Sequential-Adapt layer can control the specific size of the convolution kernel to adjust the convolution receptive field to ensure that it can fully accommodate all the feature

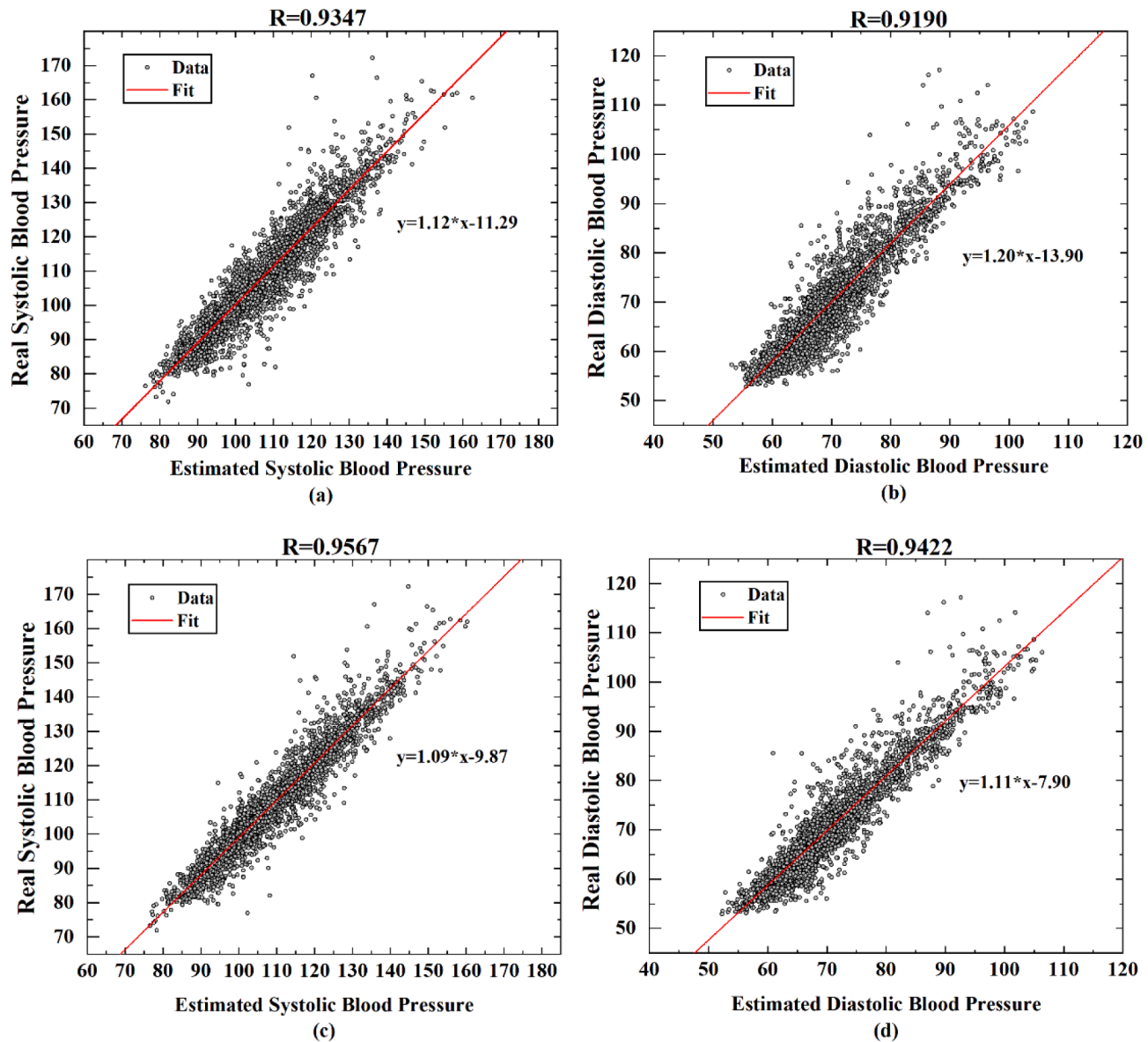


Fig. 6. The regression plots for (a) SBP and (B) DBP without SE block (upper) and (C) SBP and (d) DBP with SE block (lower) are shown above. The correlation coefficients are plotted at the top of each plot and the red line in the plot is the linear fit to the predicted point.

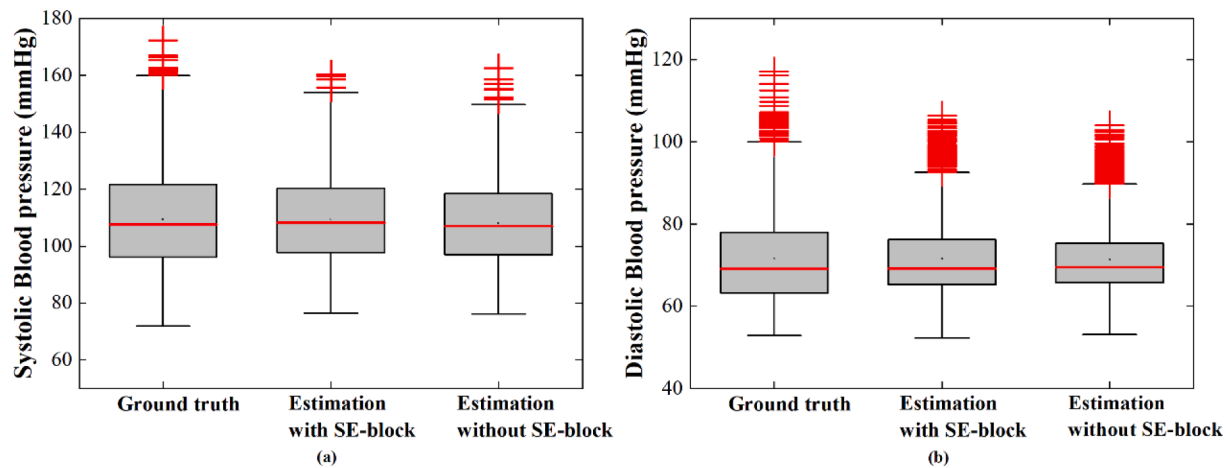


Fig. 7. The boxes plot for the ground truth of (a) SBP and (b) DBP, the estimation with and without SE block.

Table 5

Comparison of statistics with previous works.

Model	Year	Subject	Systolic Blood Pressure					Diastolic Blood Pressure				
			ME	RMSE	STD	MAE	R	ME	RMSE	STD	MAE	R
Machine Learning												
SVM [17]	2015	851	–	–	16.17	12.38	–	–	–	8.45	6.34	–
Regression [19]	2016	27	–0.37	–	5.21	–	0.91	–0.08	–	4.06	–	0.89
AdaBoost [18]	2017	942	–	–	10.09	11.17	0.59	–	–	6.14	5.35	0.48
Linear Regression [20]	2018	22	0.81	–	0.95	–	–	0.75	–	0.54	–	–
XGBoost[24]	2020	294	–	–	5.21	2.80	0.98	–	–	3.37	1.77	0.97
Deep Learning												
ResNet[28]	2019	510	–	–	–	6.88	–	–	–	–	9.43	–
ANN-LSTM [27]	2019	39	–	1.56	–	1.10	0.99	–	0.85	–	0.58	0.99
CNN-LSTM [29]	2020	200	1.91	–	5.55	–	0.95	0.67	–	2.84	–	0.95
CNN-GRU-Attention[30]	2020	15	–	4.04	–	4.06	–	–	3.42	–	3.33	–
Seq2seq-Attention[31]	2021	1131	–	15.96	15.67	12.08	–	–	7.4	7.32	5.56	–
Proposed model	2021	1216	0.18	–	5.11	3.70	0.96	0.01	–	3.95	2.81	0.94
		40	–0.35		1.71	1.37	0.99	0.05		1.18	0.93	0.99

information. Renet25_BP layer improves the overfitting phenomenon caused by the more layers and adjusts the specific pooling type by modifying ResNet. The structure of Renet25_BP is the main module that absorbs the characteristics of the input information, and its specific parameters are given in Table 1. The SE block enhances the feature extraction capability of the previous layer by reassigning the channel features. As can be seen from Table 2, when $J = 32$, after adding the SE block module to the residual block, the MAE value of SBP is reduced from 4.69 mmHg to 3.70 mmHg, and the MAE value of DBP is reduced from 3.53 mmHg to 2.81 mmHg. Furthermore, Fig. 4 shows that the lower limit of DBP is around 50 mmHg and the upper limit of SBP is 165 mmHg, which is determined by the range of the ground truth in training set. Therefore, the accuracy of the model should be reconsidered when facing the cases beyond this range.

We showed that the model with SE block has a good contribution to the feature extraction ability of PPG and ECG signals. This also proves that the model with SE block effectively extracts the eigenvalues of the model. The proposed model only depends on the input signals at the current moment, which can be used to estimate BP completely relying on the graph characteristics of the signals. For practical application, the output response speed is faster, and in the situation for patients with unstable input signals, the network structure based on graph information is more reliable.

5. Conclusion

The deep learning model based on graph information proposed for BP prediction in this paper is more effective in the performance of the database with more subjects. The previous researches on the extraction of PPG and ECG features with ML methods indicate that the biological signals such as PPG and ECG have more graph information to be mined. The accuracy of BP prediction can be significantly improved by adding CNN modules and SE block in deep learning model to promote the feature extraction ability. The outputs of the proposed model meet the AAMI criteria and the BHS A rating.

The cuffless BP measurement can continuously detect the dynamic BP values, and the deep learning methods based on the graph information extraction are more stable and adaptive for database with large subjects. Such convenient and painless BP predication method with easy-to-detect in vitro biological signals through intelligent wearable devices used in daily life will be widely applied in various fields of life, such as medical treatment, sports [41]. We believe that CVDs can be effectively prevented in the near future with the continuous detection of BP based on the combination of the wearable hardware and deep-learning algorithms.

CRediT authorship contribution statement

Ye Qiu: Conceptualization, Methodology, Software, Formal analysis, Writing - original draft. **Dongdong Liu:** Data curation, Witing - review & editing. **Guoyu Yang:** Witing - review & editing. **Dezhen Qi:** Writing - review & editing. **Yuer Lu:** Validation. **Qingzu He:** Investigation. **Xiangyu Qian:** Resources. **Xiang Li:** Visualization. **Jianwei Shuai:** Supervision, Project administration.

Declaration of Competing Interest

The authors declare that they have no known competing financial interests or personal relationships that could have appeared to influence the work reported in this paper.

Acknowledgements

We acknowledge supports from the National Natural Science Foundation of China (Grant Nos. 11874310, 12090052, and 11704318), the China Postdoctoral Science Foundation (Grant No. 2016M602071), the 111 Project (Grant No. B16029) and the Fujian Province Foundation (Grant No. 2020Y4001).

References

- [1] M.E.A.M. van Kleef, W. Spiering, Hypertension: overly important but under-controlled,, Eur. J. Prevent. Cardiol. 24 (3_suppl) (2017) 36–43, <https://doi.org/10.1177/2047487317709116>.
- [2] S.S. Virani, A. Alonso, H.J. Aparicio, et al., Heart Disease and Stroke Statistics-2021 Update: A Report From the American Heart Association, Circulation 143 (2021) e254–e743, <https://doi.org/10.1161/cir.0000000000000950>.
- [3] R. Mukkamala, J.-O. Hahn, O.T. Inan, L.K. Mestha, C.-S. Kim, H. Toreyin, S. Kyal, Toward ubiquitous blood pressure monitoring via pulse transit time: theory and practice, IEEE Trans. Biomed. Eng. 62 (8) (2015) 1879–1901, <https://doi.org/10.1109/TBME.2015.2441951>.
- [4] S.S. Mousavi, M. Firouzmand, M. Charmi, M. Hemmati, M. Moghadam, Y. Ghorbani, Blood pressure estimation from appropriate and inappropriate PPG signals using a Whole-based method, Biomed. Signal Process. Control 47 (2019) 196–206, <https://doi.org/10.1016/j.bspc.2018.08.022>.
- [5] I. Sharifi, S. Goudarzi, M.B. Khodabakhshi, A novel dynamical approach in continuous cuffless blood pressure estimation based on ECG and PPG signals, Artif. Intell. Med. 97 (2019) 143–151, <https://doi.org/10.1016/j.artmed.2018.12.005>.
- [6] P.M. Nabeel, J. Jayaraj, S. Mohanasankar, Single-source PPG-based local pulse wave velocity measurement: a potential cuffless blood pressure estimation technique, Physiol. Meas. 38 (2017) 2122–2140, <https://doi.org/10.1088/1361-6579/aa9550>.
- [7] T.H. Huynh, R. Jafari, W.-Y. Chung, Noninvasive cuffless blood pressure estimation using pulse transit time and impedance plethysmography, IEEE Trans. Biomed. Eng. 66 (4) (2019) 967–976, <https://doi.org/10.1109/TBME.2018.2865751>.
- [8] R. Mukkamala, J.-O. Hahn, Toward ubiquitous blood pressure monitoring via pulse transit time: predictions on maximum calibration period and acceptable error limits, IEEE Trans. Biomed. Eng. 65 (6) (2018) 1410–1420, <https://doi.org/10.1109/TBME.2017.2756018>.

- [9] M. Singla, P. Sistla, S. Azeemuddin, Cuff-less Blood Pressure Measurement Using Supplementary ECG and PPG Features Extracted Through Wavelet Transformation, in: 2019 41st Annual International Conference of the IEEE Engineering in Medicine and Biology Society (EMBC), 2019, pp. 4628–4631. DOI:10.1109/EMBC.2019.8857709.
- [10] Y.-Z. Yoon, J.M. Kang, Y. Kwon, S. Park, S. Noh, Y. Kim, J. Park, S.W. Hwang, Cuff-less blood pressure estimation using pulse waveform analysis and pulse arrival time, *IEEE J. Biomed. Health. Inf.* 22 (4) (2018) 1068–1074, <https://doi.org/10.1109/JBHI.2017.2714674>.
- [11] S.H. Liu, S.H. Lai, J.J. Wang, et al., The Cuffless Blood Pressure Measurement with Multi-dimension Regression Model based on Characteristics of Pulse Waveform, in: 2019 41st Annual International Conference of the IEEE Engineering in Medicine and Biology Society (EMBC), 2019, pp. 6838–6841. DOI:10.1109/EMBC.2019.8856749.
- [12] Y. Li, Z. Wang, L. Zhang, X. Yang, J. Song, Characters available in photoplethysmogram for blood pressure estimation: beyond the pulse transit time, *Australas. Phys. Eng. Sci. Med.* 37 (2) (2014) 367–376, <https://doi.org/10.1007/s13246-014-0269-6>.
- [13] H. Shin, S.D. Min, Feasibility study for the non-invasive blood pressure estimation based on ppg morphology: normotensive subject study, *Biomed. Eng. Online* 16 (1) (2017), <https://doi.org/10.1186/s12938-016-0302-y>.
- [14] E. Martinez-Ríos, L. Montesinos, M. Alfaro-Ponce, L. Peccia, A review of machine learning in hypertension detection and blood pressure estimation based on clinical and physiological data, *Biomed. Signal Process. Control* 68 (2021) 102813, <https://doi.org/10.1016/j.bspc.2021.102813>.
- [15] M. Forouzanfar, S. Ahmad, I. Batkin, H.R. Dajani, V.Z. Groza, M. Bolic, Model-based mean arterial pressure estimation using simultaneous electrocardiogram and oscillometric blood pressure measurements, *IEEE Trans. Instrum. Meas.* 64 (9) (2015) 2443–2452, <https://doi.org/10.1109/TIM.2015.2412000>.
- [16] G. Thambiraj, U. Gandhi, U. Mangalanathan, V.J.M. Jose, M. Anand, Investigation on the effect of Womersley number, ECG and PPG features for cuff less blood pressure estimation using machine learning, *Biomed. Signal Process. Control* 60 (2020) 101942, <https://doi.org/10.1016/j.bspc.2020.101942>.
- [17] M. Kachuee, M.M. Kiani, H. Mohammadzade, et al., Cuff-less high-accuracy calibration-free blood pressure estimation using pulse transit time, in: 2015 IEEE International Symposium on Circuits and Systems (ISCAS), 2015, pp. 1006–1009, <https://doi.org/10.1109/ISCAS.2015.7168806>.
- [18] M. Kachuee, M.M. Kiani, H. Mohammadzade, M. Shabany, Cuffless blood pressure estimation algorithms for continuous health-care monitoring, *IEEE Trans. Biomed. Eng.* 64 (4) (2017) 859–869, <https://doi.org/10.1109/tbme.2016.2580904>.
- [19] X.-R. Ding, Y.-T. Zhang, J. Liu, W.-X. Dai, H.K. Tsang, Continuous cuffless blood pressure estimation using pulse transit time and photoplethysmogram intensity ratio, *IEEE Trans. Biomed. Eng.* 63 (5) (2016) 964–972, <https://doi.org/10.1109/tbme.2015.2480679>.
- [20] W.-H. Lin, H. Wang, O.W. Samuel, et al., New photoplethysmogram indicators for improving cuffless and continuous blood pressure estimation accuracy, *Physiol. Meas.* 39 (2018), <https://doi.org/10.1088/1361-6579/aaa454>.
- [21] J. Feng, Z. Huang, C. Zhou, X. Ye, Study of continuous blood pressure estimation based on pulse transit time, heart rate and photoplethysmography-derived hemodynamic covariates, *Australas. Phys. Eng. Sci. Med.* 41 (2) (2018) 403–413, <https://doi.org/10.1007/s13246-018-0637-8>.
- [22] A. Hassani, A.H. Foruzan, Improved PPG-based estimation of the blood pressure using latent space features, *SIViP* 13 (6) (2019) 1141–1147, <https://doi.org/10.1007/s11760-019-01460-1>.
- [23] C. El-Hajj, P.A. Kyriacou, A review of machine learning techniques in photoplethysmography for the non-invasive cuff-less measurement of blood pressure, *Biomed. Signal Process. Control* 58 (2020) 101870, <https://doi.org/10.1016/j.bspc.2020.101870>.
- [24] Q. Hu, X. Deng, A. Wang, et al., A novel method for continuous blood pressure estimation based on a single-channel photoplethysmogram signal, *Physiol. Meas.* 41 (2021) 125009, <https://doi.org/10.1088/1361-6579/abc8dd>.
- [25] F. Miao, N. Fu, Y.-T. Zhang, X.-R. Ding, X.i. Hong, Q. He, Y.e. Li, A novel continuous blood pressure estimation approach based on data mining techniques, *IEEE J. Biomed. Health. Inf.* 21 (6) (2017) 1730–1740, <https://doi.org/10.1109/jbhi.2017.2691715>.
- [26] Y. Zhang, Z. Wang, A hybrid model for blood pressure prediction from a PPG signal based on MIV and GA-BP neural network, in: 2017 13th International Conference on Natural Computation, Fuzzy Systems and Knowledge Discovery (ICNC-FSKD), 2017, pp. 1989–1993, <https://doi.org/10.1109/ICNC-FSKD.2017.8393073>.
- [27] M.S. Tanveer, M.K. Hasan, Cuffless blood pressure estimation from electrocardiogram and photoplethysmogram using waveform based ANN-LSTM network, *Biomed. Signal Process. Control* 51 (2019) 382–392, <https://doi.org/10.1016/j.bspc.2019.02.028>.
- [28] G. Slapničar, N. Mlakar, M. Luštrek, Blood Pressure Estimation from Photoplethysmogram Using a Spectro-Temporal Deep Neural Network, *Sensors* (Basel, Switzerland) 19 (2019), <https://doi.org/10.3390/s19153420>.
- [29] J. Esmaelpoor, M.H. Moradi, A. Kadkhodamohammadi, A multistage deep neural network model for blood pressure estimation using photoplethysmogram signals, *Comput. Biol. Med.* 120 (2020) 103719, <https://doi.org/10.1016/j.compbiomed.2020.103719>.
- [30] H. Eom, D. Lee, S. Han, Y.S. Hariyani, Y. Lim, I. Sohn, K. Park, C. Park, End-to-end deep learning architecture for continuous blood pressure estimation using attention mechanism, *Sensors* 20 (8) (2020) 2338, <https://doi.org/10.3390/s20082338>.
- [31] N. Aguirre, E. Grall-Maës, L.J. Cymberknop, R.L. Armentano, Blood pressure morphology assessment from photoplethysmogram and demographic information using deep learning with attention mechanism, *Sensors* 21 (6) (2021) 2167, <https://doi.org/10.3390/s21062167>.
- [32] O. Erkaymaz, M. Ozer, M. Perc, Performance of small-world feedforward neural networks for the diagnosis of diabetes, *Appl. Math. Comput.* 311 (2017) 22–28, <https://doi.org/10.1016/j.amc.2017.05.010>.
- [33] Y. Isler, A. Narin, M. Ozer, M. Perc, Multi-stage classification of congestive heart failure based on short-term heart rate variability, *Chaos, Solitons Fractals* 118 (2019) 145–151, <https://doi.org/10.1016/j.chaos.2018.11.020>.
- [34] M. Saeed, M. Villarroel, A.T. Reisner, G. Clifford, L.-W. Lehman, G. Moody, T. Heldt, T.H. Kyaw, B. Moody, R.G. Mark, Multiparameter Intelligent Monitoring in Intensive Care II: a public-access intensive care unit database, *Crit. Care Med.* 39 (5) (2011) 952–960, <https://doi.org/10.1097/CCM.0b013e31820a92c6>.
- [35] X. Qin, X. Zha, J. Huang, et al., Radar Waveform Recognition based on Deep Residual Network, in: 2019 IEEE 8th Joint International Information Technology and Artificial Intelligence Conference (ITAIC), 2019, pp. 892–896, <https://doi.org/10.1109/ITAIC.2019.8785588>.
- [36] S. Hershey, S. Chaudhuri, D.P.W. Ellis, et al., CNN architectures for large-scale audio classification, in: 2017 IEEE International Conference on Acoustics, Speech and Signal Processing (ICASSP), 2017, pp. 131–135, <https://doi.org/10.1109/ICASSP.2017.7952132>.
- [37] K. He, X. Zhang, S. Ren, et al., in: Deep Residual Learning for Image Recognition, IEEE, 2016, pp. 770–778, <https://doi.org/10.1109/CVPR.2016.90>.
- [38] J. Hu, L.i. Shen, S. Albanie, G. Sun, E. Wu, Squeeze-and-Excitation Networks, *IEEE Trans. Pattern Anal. Mach. Intell.* 42 (8) (2020) 2011–2023, <https://doi.org/10.1109/TPAMI.2019.2913372>.
- [39] X. Xing, M. Sun, Optical blood pressure estimation with photoplethysmography and FFT-based neural networks, *Biomedical Opt. Express* 7 (8) (2016) 3007, <https://doi.org/10.1364/BOE.7.003007>.
- [40] E. O??Brien, J. Petrie, W. Littler, M. de Swiet, P.L. Padfield, K. O??Malley, M. Jamieson, D. Altman, M. Bland, N. Atkins, The British Hypertension Society protocol for the evaluation of automated and semi-automated blood pressure measuring devices with special reference to ambulatory systems, *J. Hypertens.* 8 (7) (1990) 607–619, <https://doi.org/10.1097/00004872-199007000-00004>.
- [41] M. Chen, Y. Ma, J. Song, C.-F. Lai, B. Hu, Smart clothing: connecting human with clouds and big data for sustainable health monitoring, *Mobile Networks Appl.* 21 (5) (2016) 825–845, <https://doi.org/10.1007/s11036-016-0745-1>.